Shear Thickening Electrolyte Built from Sterically Stabilized Colloidal Particles

Brian H. Shen,[1,2] Beth L. Armstrong,[1] Mathieu Doucet,[3] Luke Heroux,[4] James F. Browning,[4] Michael Agamalian,[4] Wyatt E. Tenhaeff,[2] Gabriel M. Veith[1,*]

[1] Materials Science and Technology Division, Oak Ridge National Laboratory, Oak Ridge TN, 37831
[2] Department of Chemical Engineering, University of Rochester, Rochester, NY 14627
[3] Neutron Data Analysis and Visualization Division, Oak Ridge National Laboratory, Oak Ridge TN 37831
[4] Chemical and Engineering Materials Division, Oak Ridge National Laboratory, Oak Ridge TN 37831
[*] *Corresponding Author* – veithgm@ornl.gov

KEYWORDS: Shear thickening, electrolyte, steric stabilization, USANS

ABSTRACT: We demonstrate a method to prepare shear-thickening electrolytes consisting of silica nanoparticles in conventional liquid electrolytes with limited flocculation. These electrolytes rapidly and reversibly stiffen to solid-like behaviors in the presence of external shear or high impact, which is promising for improved lithium ion battery safety, especially in electric vehicles. However, in initial chemistries the silica nanoparticles aggregate and/or sediment in solution over time. Here, we demonstrate steric stabilization of silica colloids in conventional liquid electrolyte *via* surface-tethered PMMA brushes, synthesized *via* surface-initiated atom transfer radical polymerization. Ultra small angle neutron scattering revealed a reduction in aggregation of PMMA-coated silica nanoparticles compared to bare silica nanoparticles in solution under shear and at rest, suggesting good stabilization. Conductivity tests of shear thickening electrolytes (30 wt.% solids in electrolyte) at rest were performed with interdigitated electrodes over the course of 24 hours. Conductivity of electrolytes with bare silica decreased severely from 9.10 to 1.27 mS cm^{-1} as sedimentation occurred. In contrast, conductivity of electrolytes with PMMA-coated silica decreased slightly from 9.56 to a stable 7.70 mS cm^{-1} over the same time period, suggesting good colloid stability at rest.

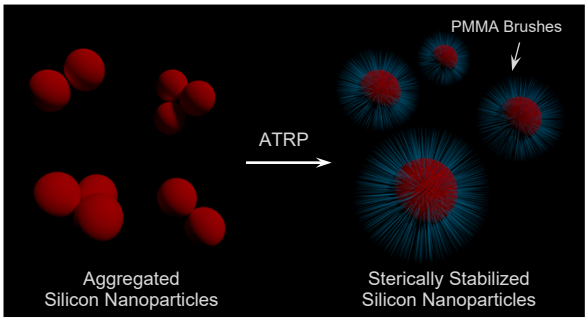

1. Introduction

Lithium ion batteries are continuously being optimized for demanding applications such as electric vehicles; however, significant safety concerns around the flammable alkyl carbonate electrolyte solvents in lithium ion batteries remain.[1] This is especially true when considering collisions involving electric vehicles that can result in electrode shorting and lead to thermal runaway and combustion of these solvents.[2] One approach to mitigating the fire hazard is the design of solid state batteries, which employ nonflammable solid ionic conductors. Ideally, the mechanical properties of the solid electrolyte can also impart additional mechanical strength to the cell. While many solid electrolytes have been designed with compelling ionic conductivities approaching or even surpassing conventional liquid electrolytes, the solid state nature requires the complete redesign of the electrochemical cell, and the efficient utilization of the conventional slurry-cast, porous composite electrodes is nontrivial to achieve.[3-4] There is strong demand for the development of safe electrolytes that can replace conventional liquid electrolytes but do not require redesign of the whole cell.[5]

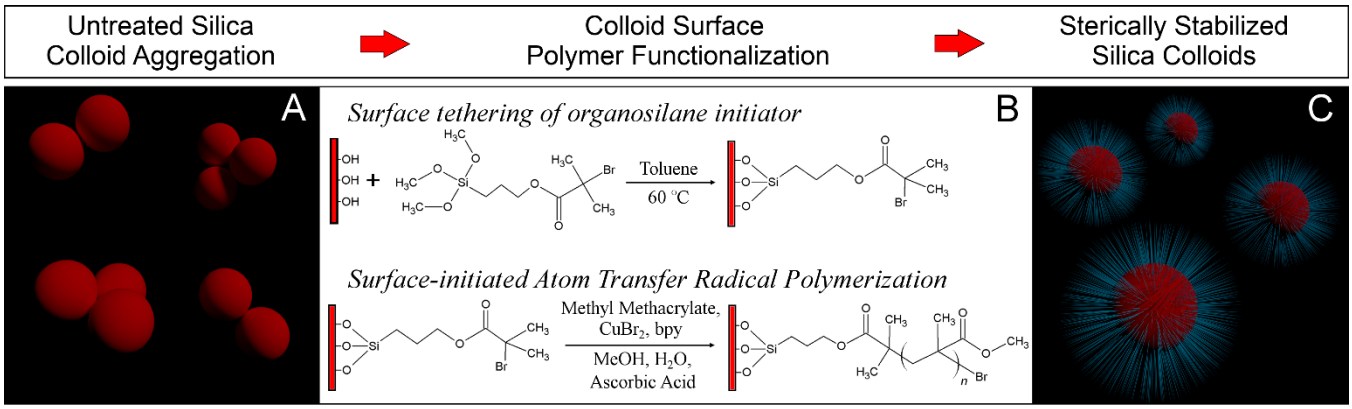

Scheme 1. A) Cartoon depiction of aggregation of bare silica nanoparticles in solution. B) Scheme depicting attachment of organosilane to silica colloid surfaces (top) and grafting of poly(methyl methacrylate) (PMMA) brushes from colloid surfaces *via* surface-initiated activators regenerated by electron transfer atom transfer radical polymerization (ARGET-ATRP) (bottom). C) Cartoon depiction of silica nanoparticles sterically stabilized *via* surface tethered PMMA brushes.

One such approach is the recent development of shear-thickening SAFe Impact Resistant Electrolytes (SAFIRE), which undergo a rapid, reversible rheological transition from liquid to solid-like viscosities upon application of external shear while maintaining the ionic conductivities required for high rate applications.[6-7] This transition to solid-like viscosities dramatically improves the safety of lithium ion batteries during an impact, such as a car crash. The rheological theory for shear-thickening behavior states that shear causes the colloids to aggregate into clusters that block fluid flow due to coulombic and surface hydrodynamic interactions at short distances between colloids.[8] However, in conventional alkyl carbonate-based electrolytes, we have observed that untreated silica colloids in suspension aggregate over time, even in quiescent conditions, and precipitate from solution.[9-12] Significant sedimentation of solid colloids would result in an electrolyte that does not exhibit any rheological response to shear. This is an especially important consideration for implementation in any practical electrochemical cell requiring long calendar lives, such as those found in consumer electronics and electric vehicles or in other materials such as the "soggy sand" electrolytes.[12-15]

We seek to reduce this sedimentation and improve dispersion stability by growing covalently-tethered polymer brushes (poly(methyl methacrylate), (PMMA)) from silica nanoparticle surfaces *via* activators regenerated by electron transfer atom transfer radical polymerization (ARGET-ATRP) to provide steric stabilization, as shown in **Scheme 1**A and 1C.[16] The chemistry for functionalization of silica surfaces is shown in Scheme 1B. Steric stabilization is a well-established approach for stabilizing colloidal dispersions.[17-20] Poly(methyl methacrylate) (PMMA) was chosen for the polymer compositions as its polymerization is well documented and has been used as a matrix in polymer gel electrolytes for lithium ion batteries.[21-22] We investigate the rheological behavior of these electrolytes *in situ* to understand how these polymers affect colloid aggregation in shear. Finally, we use these electrolytes in electrochemical cells. These findings will guide design of sterically stabilizing coatings for colloids in shear thickening electrolytes that effectively reduce aggregation at rest and enable shear thickening behavior even at long calendar times.

2.Experimental Section

2.1 Silica nanoparticle synthesis

Chemicals: Tetraethyl orthosilicate (≥ 99.0% purity, Sigma Aldrich), ammonium hydroxide (28% in H_2O, VWR), and ethanol (200 proof, Decon Labs) were purchased and used as received.

Ethanol (425mL), deionized water (50 mL), and ammonium hydroxide (50 mL) were added to a round bottom flask. The contents were chilled to 0 °C using an ice bath, after which tetraethyl orthosilicate (43 mL) was added dropwise to the round bottom flask and the contents were left to react for at least 15 hours, according to the method by Stöber.[23] The resulting precipitated silica nanoparticles were rinsed in ethanol three times. To do this, the particles were collected by centrifugation (Allegra 6, Beckman Coulter) and the supernatant was decanted. The nanoparticles were ultrasonicated (XL2010, Heat Systems Inc.) in ethanol. This process was repeated twice more before centrifuging one final time. The particles were then dried at room temperature in vacuum overnight. The silica particles were reported to be 200 nm in diameter measured by dynamic light scattering.

2.2 Silica surface functionalization

Chemicals: Toluene (anhydrous 99.8%, Sigma), silane coupling agent (3-(Trimethoxysilyl)propyl 2-bromo-2-methylpropanoate, Gelest), methanol (99.8%, VWR), methyl methacrylate (99%, ≤30 ppm MEHQ inhibitor, Sigma Aldrich), deionized water, 2,2'-bypyridine (≥99%, Sigma Aldrich), copper bromide (99%, Sigma Aldrich), ascorbic acid (reagent grade, Sigma Aldrich) were purchased and used as received, except for methyl methacrylate, which was passed through an inhibitor removal column (DH-4, Scientific Polymer Products) three times.

Silica nanoparticles were reacted with the silane coupling agent in toluene (5 µL per gram silica), with stirring at 500 rpm and 70 °C overnight. The silane treated

silica nanoparticles were rinsed with methanol three times to remove excess silane, in a similar fashion to the process used before. PMMA chains were grown on the surface *via* atom transfer radical polymerization (ATRP).[24] The silica nanoparticles were added to a solution of deionized water (8.0 ml), methyl methacrylate (40 ml), methanol (32 ml), copper bromide (14.70 mg), bipyridyl (103.1 mg), and ascorbic acid (116.2 mg). The nanoparticles were stirred in solution at 500 rpm for four hours at room temperature. The now functionalized nanoparticles were soaked in acetone overnight to ensure the PMMA was attached and not simply adsorbed on the silica surfaces. The particles were then rinsed in acetone three times before drying at room temperature in vacuum overnight.

2.3 Silica nanoparticle characterization

Thermogravimetric analysis (TGA) was performed on PMMA-coated silica nanoparticle samples using a TA Instruments Q500 TGA. Samples were analyzed on platinum pans from 30 °C to 1000 °C in nitrogen. For comparison, commercial PMMA powder was also analyzed (600 micron, extrusion grade, Goodfellow Cambridge).

Fourier transform infrared spectroscopy (FTIR) was conducted using a Bruker Alpha FT-IR spectrometer with a diffuse reflectance infrared Fourier transform spectroscopy (DRIFTS) attachment. PMMA-coated silica nanoparticles were compared to bare silica nanoparticles and commercial PMMA powder.

Zeta potential measurements were conducted on silica nanoparticles, bare or PMMA-coated, in dilute aqueous solutions using a zeta potential analyzer (Brookhaven Instruments, ZetaPals). To prepare these solutions at the correct dilutions (order of 10^{-6} wt. %) appropriate amounts of particles were added to deionized water and KNO_3 (0.01M). Solutions were titrated across a range of pH (2-10) using HNO_3 (1M) and HN_4OH (1M).

2.4 Scanning Electron Microscopy

Bare and PMMA-coated silica nanoparticles were dispersed in ethanol and coated on to a copper grid. They were imaged using a Hitachi S-3400 scanning electron microscope with variable pressure operated between 10 and 15 kV.

2.5 Rheology

Rheological measurements were conducted on shear-thickening electrolyte solutions using a rheometer (Physica MCR501, Anton Paar) fitted with a concentric cylinder geometry. Solutions were prepared by adding appropriate amounts of nanoparticles, bare of PMMA-coated, in propylene carbonate. Solutions were hand mixed as the shear-thickening behavior of the solutions prevented mixing by other techniques. Propylene carbonate was chosen instead of other conventional lithium ion battery electrolytes such as ethylene carbonate (EC) or dimethyl carbonate (DMC) for its low vapor pressure as the solutions will be exposed to air for long times. For most samples, titanium outer (50mm diameter) and inner (48mm diameter) cylinders were used. Quartz outer (50mm diameter) and inner (49mm diameter) cylinders were used for solutions to be analyzed with ultra-small-angle neutron scattering. Solutions were conditioned with a low shear rate (5 s^{-1}) for 30 seconds to disperse agglomerated particles and were allowed to equilibrate for one minute prior to measurements. Variable rate measurements were conducted at rotation rates ranging from 0 to 100 s^{-1}. Constant rate measurements were conducted at rotation rates where shear-thickening behavior was most prominent. All rheological measurements were conducted at room temperature.

2.6 Ultra Small-Angle Neutron Scattering (USANS)

Neutron data was collected at the USANS instrument at Oak Ridge National Laboratory's Spallation Neutron Sources (SNS). USANS was chosen as it can analyze the large 200 nm diameter silica colloids in solution. The USANS instrument is a time-of-flight triple-bounce Bose-Hart small-angle scattering instrument that allows measurements down to 10^{-6} in Q.[25] The data was acquired using the 3.6 Angstrom reflection of the analyzer crystals. This provided a minimum Q of 0.0001 $Å^{-1}$, which is enough to cover the whole signal from our sample. The raw data was reduced using the Mantid framework to compute I(Q).[26] For each sample run, a background run with only propylene carbonate was taken in the same conditions. The I(Q) distribution from the background was subtracted from the sample I(Q). The 1 wt. % data was modelled using the SasView small-angle scattering software package.[27]

2.7 Electrochemistry

Coin cells were assembled using graphite and $LiNi_{1/3}Mn_{1/3}Co_{1/3}O_2$ (NMC) electrodes in a balanced full cell configuration. The graphite and NMC electrode active-material areal densities were 9 and 19.95 mg/cm^2, respectively. Two separators (Gold 40, Dreamweaver) were used and 100 µL electrolyte was added (1.2M $LiPF_6$ in 3:7 EC:DMC, BASF). The electrodes and separators were dried at 120 °C before use. Shear-thickening electrolytes for the coin cells were prepared to a target concentration of 30% solids by weight in liquid electrolyte. At such high loadings, the shear-thickening electrolytes easily transition to almost solid like behaviors with very little shear. The electrolytes were slowly mixed by hand using a glass stirring rod. Two plastic spatulas were used to portion the electrolyte between the two separators. Electrochemical cycling was conducted using a battery cycler (Series 4000, Maccor) at a rate of C/3 from 3.0V to 4.2V at room temperature.

To understand how sedimentation affects ionic conductivity, interdigitated electrodes (IDEs, cell constant 2 cm^{-1}, model CC1.W, BVT Technologies) were submerged in solutions of 30 wt.% solids in 1.0M $LiPF_6$ 1:1 EC/DMC v/v electrolyte. Wires connected to the IDEs were threaded through the top of a butyl 20 mL scintillation vial cap and sealed with epoxy. The shear thickening electrolyte solutions were prepared by hand-mixing in Ar(g) in 20 mL scintillation vials. The vials were sealed with the modified cap with IDE. The IDEs were then connected to a potentiostat (SP300, BioLogic Science Instruments). Conductivity was measured at 25 °C at 871 kHz, 108 kHz, and 435 kHz, for electrolytes with no silica, bare silica, and

PMMA-coated silica, respectively. The IDEs were positioned 1 mm from the bottom of the vial to measure the conductivity of the colloid sediment over time.

3. Results and Discussion

3.1 Characterization of Silica with Surface-Tethered PMMA Brushes

To measure the amount of PMMA tethered to the silica nanoparticles, thermogravimetric analysis (TGA) was conducted on PMMA-coated silica nanoparticles and commercial PMMA for comparison. TGA data for these materials are shown in **Figure 1**. Initially, loosely bound water leaves the surface from 30 to 190 °C, as evident in the decrease in weight. Subsequently, a tightly bound water layer leaves the surface beginning at 190 °C.[28] A 37.03% drop in mass is observed for treated particles beginning at 285 °C and ending at approximately 400°C. This closely matches the decomposition observed for commercial PMMA beginning at 285.7 °C and ending at 391.9 °C. This suggests the loss of mass observed in functionalized silica colloids can be attributed to the decomposition of PMMA on their surfaces.

The observed mass loss in treated particles was used to estimate individual chain length. Assuming each individual PMMA chain occupies 1.2 nm^2 of the surface of a silica nanoparticle each chain is 78.6 nm in length.[29-30] Additional losses are observed for treated particles. Slight loss in weight after 400 °C may indicate the degradation of the organosilane used to tether the polymer to the silica nanoparticle surface.

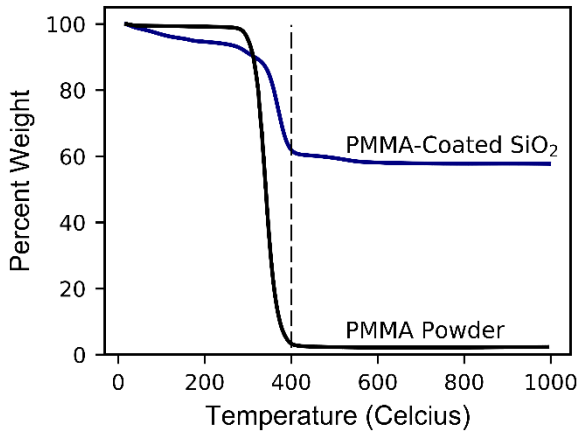

Figure 1. Thermogravimetric analysis data of PMMA-coated silica colloids and commercial PMMA powder. Samples were analyzed in platinum pans in N_2 from 35 to 1000 °C

Diffuse reflectance infrared Fourier transform spectroscopy (DRIFTS) was performed to understand the surface composition of PMMA-coated silica nanoparticles. **Figure 2** shows representative DRIFTS data collected on bare silica, PMMA-coated silica, and commercial PMMA powder for comparison. Peaks are observed in the spectrum for silica nanoparticles at 1070 and 458 cm^{-1}, which can be attributed to Si-O-Si stretching and Si-O deformation, respectively.[31] A small band is observed at 2990 cm^{-1} in the treated silica spectrum, which can be attributed to a C-H stretch from the methoxy and methyl groups in PMMA. The peak observed at 1728 cm^{-1} in both the commercial PMMA and treated silica spectra is characteristic of PMMA and is attributed to an acrylate carboxyl functional group.[32] Two bands, 1390 and 754 cm^{-1}, can be attributed to methyl group vibrations. A band is seen from 1040 - 1260 cm^{-1} and can be attributed to a $-OCH_3$ stretching vibration. These peaks closely correspond with the spectrum obtained from analysis of commercial PMMA powder, confirming that the silica nanoparticles are covered with PMMA.

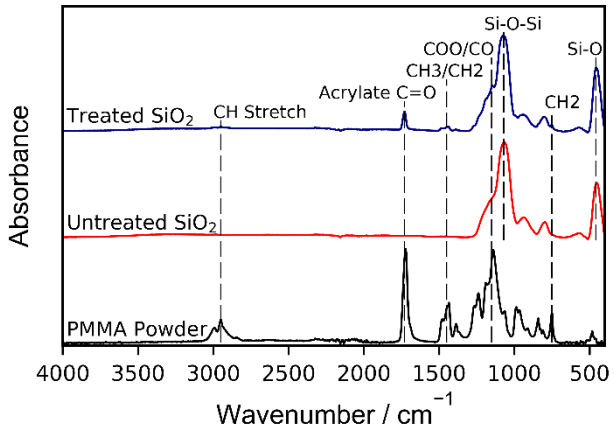

Figure 2. DRIFTS spectra for treated and bare silica, as well as commercial PMMA for comparison.

It is important to reiterate that the treated particles were rinsed and soaked overnight in acetone- a good solvent for PMMA. Thus, it is unlikely that there are free PMMA chains adsorbed on silica nanoparticle surfaces. From these data, we can conclude that the PMMA brushes are covalently bound to the silica nanoparticle surfaces and remain tethered to the silica surface in solvent. Both attributes are a benefit to shear-thickening electrolytes, as long term stability is desirable for proper response to shear.

To qualitatively evaluate differences in aggregation behavior of bare and PMMA-coated silica nanoparticles, scanning electron microscopy (SEM) was performed on dry powders. Micrographs of bare and PMMA-coated silica nanoparticles are shown in **Figure 3A** and **Figure 3B**, respectively. Bare silica nanoparticles are observed to be aggregated into small networks as expected. In contrast, PMMA-coated nanoparticles appear to remain more evenly dispersed, suggesting the PMMA surface-tethered brushes aid in sterically stabilizing the particles and reducing aggregation.

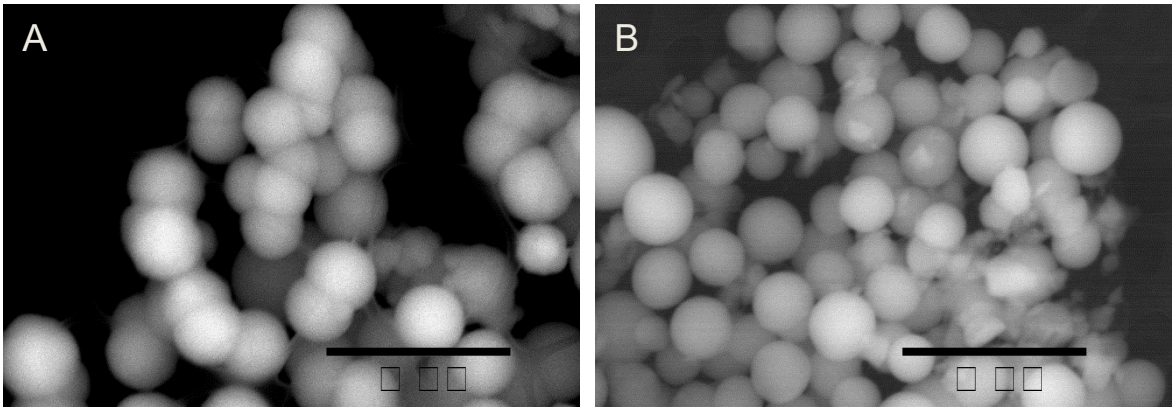

Figure 3. Micrographs of A) bare and B) PMMA-coated silica nanoparticles.

3.2. Rheological behavior

The rheological behavior of the silica nanoparticles (bare and PMMA-coated) was characterized in propylene carbonate (a common solvent in lithium ion battery electrolytes), and the critical solid loadings in the colloidal dispersions for shear-thickening behavior was determined. **Figure 3** shows rheology data as a function of weight loading for solutions ranging from 0 – 15 wt.% PMMA-coated nanoparticles. A transition from Newtonian to non-Newtonian, shear-thickening behavior is observed between 10 - 15 wt.% loading similar to what was reported previously for uncoated materials.[7] In solutions up to 10 wt. % solids loading, the viscosities remain relatively constant despite increasing shear rate and have linear rate/stress curves, suggesting Newtonian behavior. The viscosity of the 15 wt.% nearly doubles as shear rate approaches 100 s^{-1}, as shown in Figure 3b; in addition, a subtle, rising inflection is observed in the stress/rate curve of the 15wt.% solution, as shown in **Figure 4**a. Both properties suggest shear-thickening behavior was observed for solutions greater than 15 wt.%.

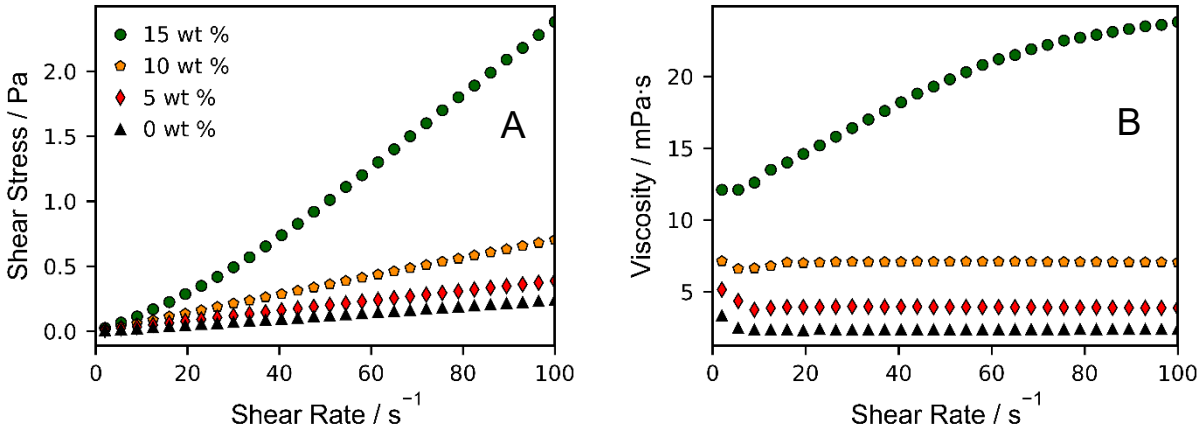

Figure 4. A) Shear stress and B) viscosity as a function of shear rate for solutions of various loadings of PMMA-coated silica colloids in propylene carbonate.

Typically, during a rheological experiment of a shear thickening slurry, particle sediment can be redistributed into the bulk using a starch pasting cell fixture. Neutron measurement limitations forced use of a concentric cylinder attachment instead, and thus sedimentation was prone to occur more quickly within the timeframe of the experiment. However, this was fortuitous, as this allowed us to compare the sedimentation rate or stability of shear-thickening electrolytes containing bare or PMMA-coated silica nanoparticles. To qualitatively compare the long-term stability of shear-thickening fluid under constant shear, two 30 wt.% solutions were prepared using either treated or bare silica nanoparticles. The treated particle solution was sheared at 50 s^{-1}, and the bare particle solution was sheared at 16.7 s^{-1}. The rates were chosen based on regimes where the rate of viscosity increase was highest. The solutions were sheared for 24 hours to determine whether the particles remain evenly dispersed in solution or aggregate and precipitate from solution. Viscosity data as a function of time is shown in **Figure 5**. It is observed that the decline in viscosity of the solution containing treated silica particles under constant shear is less severe than that of solutions with bare silica. After 24 hours, electrolyte viscosity containing bare silica colloids reaches 51.7% of initial viscosity, compared with 76.7% in electrolyte with PMMA-coated silica colloids. Moreover, viscosity of the dispersion containing PMMA-coated nanoparticles appears to stabilize at around 15 hours with a flatter slope, whereas the viscosity of the bare nanoparticle dispersion appears to continue to decay after 24 hours. This confirms that polymer treatment of silica nanoparticles helped to stabilize the particle dispersion.

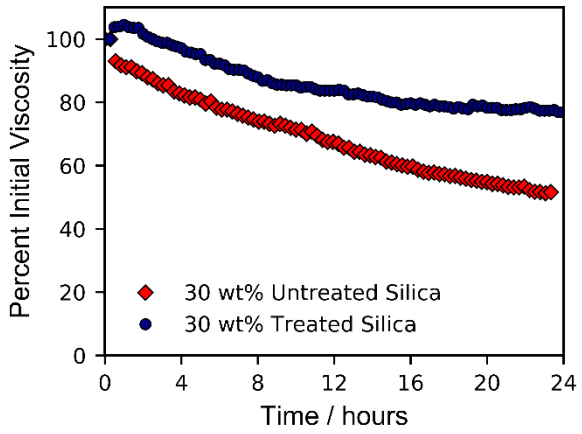

Figure 5. Viscosity of silica nanoparticle dispersion in propylene carbonate measured as a function of time.

3.2.1 Zeta Potential

Additional characterization methods were used to further understand interfacial interactions. Zeta potentials were measured to understand how the polymer treatment affecting particle-particle interactions at rest. Dilute (1 wt.%) solutions of silica nanoparticles, PMMA-coated or bare, in aqueous solutions were analyzed for zeta potential. **Figure 6** shows zeta potential data for PMMA-coated and bare particles in solution. For bare particles, the isoelectric point is moderately low, pH (~3), followed by > 40 mV increase in the magnitude of the potential at higher pH. Initially, the surface hydroxyls remain stable in solution. However, as pH increases, the presence of hydroxides interfere with silica surface silanols, forming a mixture of Si-OH/Si-O^- termination groups. More ionized silanols initiate bridging between particles, leading to increased aggregation.[10, 33] For PMMA-coated particles with PMMA, similar zeta potential behavior is observed at low pH. However, as pH increases, the zeta potential is observed to be lower in magnitude compared to that of bare silica nanoparticles. This suggests that the silica surfaces are more neutral as pH approaches 6-8, and the plane of shear is further from the nanoparticle surfaces.[34-35] This would suggest the presence of PMMA on the silica surface, and confirm that the PMMA is sterically stabilizing the particles, reducing aggregation at higher pH. It is important to note that the zeta potential for PMMA-coated nanoparticles at greater pH (6, >8), though smaller in magnitude than that of bare nanoparticles, is still rather high. This suggests that despite the large brush network covering the surface of PMMA-coated nanoparticles, a sufficient amount of surface is exposed to initiate some aggregation, as mentioned above. Because the PMMA initiation sites rely on siloxane bond chemistry, it is unlikely that the entire particle surface is covered in brushes, supported by the loss of tightly bound water in the TGA results as well as evidence of some surface charge in the zeta potential results. This is desirable, as shear-thickening behavior can be maintained. These results suggest that the PMMA brushes are effective in reducing aggregation and improving nanoparticle stability/dispersion, but not so much as to prevent shear-thickening behavior altogether.

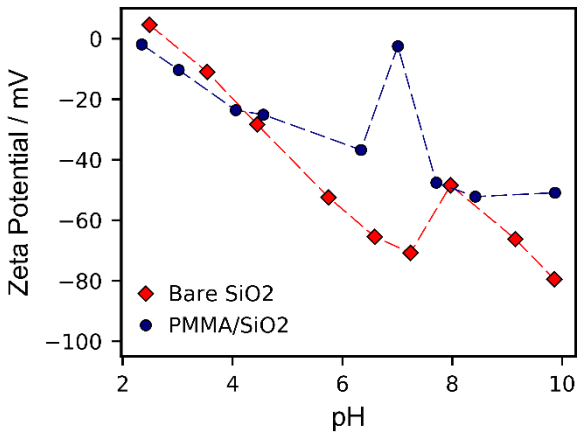

Figure 6. Zeta potential data for dilute solutions of silica colloids (bare or PMMA-coated) in deionized water. Solutions were titrated using 1M HNO_3 and 1M HN_4OH. Dashed lines are included only to show trends.

3.2.2 Ultra small angle neutron scattering

Ultra small angle neutron scattering (USANS) was performed on solutions with PMMA-coated and bare particles to understand the degree to which the respective particles aggregate in quiescent media and under shear. USANS measures scattering length density variations for large structures in solution. Specifically, while zeta potential and rheology reveals general aggregation trends, USANS provides average aggregate size and surface features. Initially, low loading solutions (1 wt.% concentration in propylene carbonate) were analyzed using bare and PMMA-coated or bare silica nanoparticles. The sample cuvettes were rotated to promote good mixing. **Figure 7** shows USANS data for these solutions of PMMA-coated and bare particles. The solid lines show a representative fit of the data. A greater intensity is observed in 1 wt. % solutions with bare particles in the range of $Q \sim 10^{-4}$ than those with PMMA-coated particles. This implies that bare solids have a greater diameter than PMMA-coated solids. Originally this was thought counterintuitive, as the PMMA-coated particles should have a greater volume with the addition of PMMA brushes, resulting in a greater intensity. It is more likely, however, that particles will not be isolated and small agglomerates will form in solution. Thus, the greater intensity in the bare particle data suggests that the aggregate size of bare particles in solution is greater than that of PMMA-coated particles. This is consistent with rheological data and zeta potential data, and shows that the PMMA treatments aids in stabilizing particles in equilibrium. Fitting reveals an average radius of bare nanoparticle agglomerates of 5060 ± 70 Å and an average radius of PMMA-coated nanoparticle agglomerates of 4034 ± 125 Å. Thus, the volume of aggregates with bare particles is approximately twice as large as those with PMMA-coated particles, suggesting that the PMMA-coated silica nanoparticles are less likely to aggregate in suspension, supporting the use of PMMA brushes as a steric stabilizer in solution.

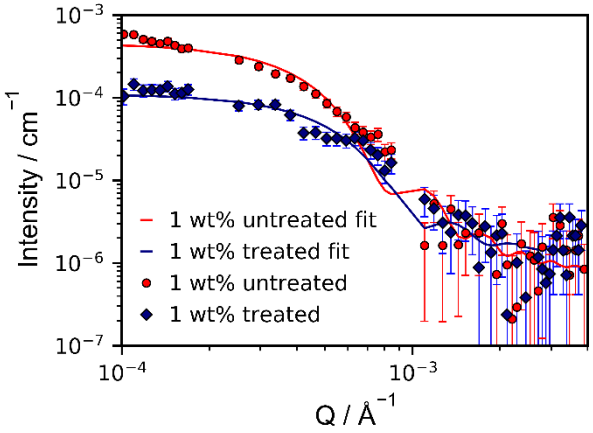

Figure 7. Markers show USANS data for 1 wt.% bare and PMMA-coated silica particles in propylene carbonate. Fitting is represented by solid lines.

USANS investigations of higher concentration (15 wt. %) shear-thickening electrolytes at rest and under shear using a rheometer were also performed. Use of the concentric cylinder rheometer attachments due to USANS sampling requirements encouraged sedimentation of bare silica nanoparticles so quickly, we opted to limit solids concentrations to 15 wt.%. USANS was performed on the solutions first at rest, then under shear (60 s^{-1}) for the duration of the procedure. **Figure 8** shows the USANS data collected for solutions containing PMMA-coated or bare particles, at rest and under shear. The largest decrease in USANS intensity for solutions with PMMA-coated particles has a flatter slope than that of solutions with bare particles. This suggests that in solutions with PMMA-coated particles, the agglomerate surfaces have some surface roughness, while those in solutions with bare particles are smoother. This is in agreement with prior characterization that demonstrates the presence of the PMMA brushes on the surface of PMMA-coated particles.

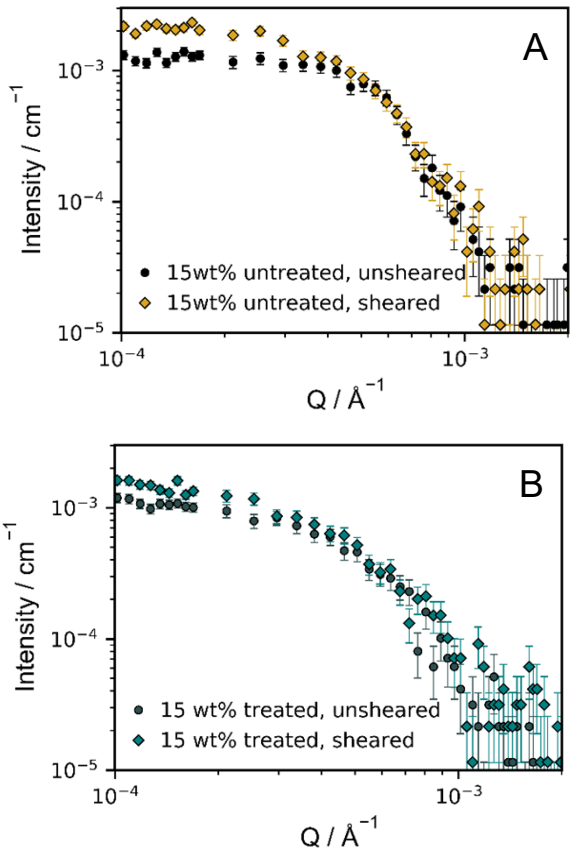

Figure 8. A) USANS data of bare silica nanoparticles for at rest (black circles) and under shear (gold diamonds). B) USANS data of 15% PMMA-coated silica nanoparticles for at rest (dark-green circles) and under shear (teal diamonds)

The intensity increases slightly under shear in solutions with bare particles (from ca. 1.1 to 2.2*10^{-3} cm^{-1}) and PMMA-coated particles (from ca. 1.1 to 1.6*10^{-3} cm^{-1}), as was expected in Figure 8. This is attributed to an increase in particle aggregation as generally observed in sheared dilatants.[36-37] As with the results from Figure 7, the increase

in intensity is smaller in sheared solutions with PMMA-coated particles than that of solutions with bare particles. Likely the aggregation of particles in solution with PMMA-coated particles is smaller than that of bare particles, further confirming that the PMMA brushes act to sterically stabilize the silica nanoparticle surfaces without completely negating shear-thickening effects. While aggregation behavior is lesser with PMMA-coated particles, the shear imparted by vehicle collisions will elicit a much greater shear-thickening response than at the shear rates used experimentally. The USANS results also suggest lower tendency to aggregate, which will yield more evenly dispersed particles in solution for longer periods of time. For many electrochemical applications, this is a great benefit, as the solutions would exhibit shear-thickening behaviors even after long calendar times.

3.3 Stability During Electrochemical Cycling

To verify the viability of these colloidal dispersions as shear thickening electrolytes, their influence on the cycling performance of lithium ion cell was assessed. Electrochemical full cells consisting of graphite anodes and $LiNi_{1/3}Mn_{1/3}Co_{1/3}O_2$ (NMC) were cycled galvanostatically at a C/3 rate (based on the capacity of the cathode). **Figure 9** shows cycling data for coin cells with and without shear thickening electrolyte. The shear thickening electrolyte was 30 wt.% solids, which were either PMMA-coated or bare silica. In electrochemical cells using conventional ethylene carbonate (EC) and dimethyl carbonate (DMC) solvent based lithium ion battery electrolytes (1.2M $LiPF_6$ 3:7 EC:DMC) without silica nanoparticles, a steady reversible charge capacity of 141 mAh g^{-1} was observed over 100 cycles. The coulombic efficiency stabilizes to 99.94 ± 2.29% which is due to a stable SEI and indicates less capacity loss to continual degradation of the electrolyte. This behavior is consistent with other studies of NMC, and was used as a baseline to compare the cells employing the shear thickening electrolytes.[38]

Capacity is observed to be lower in cells with shear-thickening electrolyte containing PMMA-coated silica nanoparticles starting with 140 mAh g^{-1} reversible capacity and ending with 122 mAh g^{-1}. The slightly better performance is certainly due in part to the aforementioned effects of high electrolyte viscosity and non-ionically conducting silica. Average coulombic efficiency (excluding first cycle) was 99.78 ± 0.21% The additional slight loss in capacity can be attributed to the presence of electrically insulating PMMA brushes on the surface of the silica nanoparticles, which are non-ionically conductive. The similar decline in capacity can also be attributed exposed silica nanoparticle surfaces, introducing water into the electrolyte.

Cells with electrolyte containing bare silica nanoparticles have the lowest capacities starting with a discharge capacity of 126 mAh g^{-1} and ending at 108 mAh g^{-1} after 100 cycles. The loss in capacity can be explained by the introduction of non-ionically conducting silica nanoparticles, hindering ion mobility, as well as the Nernst-Einstein equation, showing that ionic conductivity is inversely proportional to viscosity, which in turn is proportional to concentration.[39] Previous comparisons of conventional and shear-thickening electrolytes show that ionic conductivity is lower in the dispersions.[7] Average coulombic efficiency (excluding first cycle) was 99.85 ± 0.32%. The steady decline in capacity over time is most likely attributed to the presence of tightly bound water on the surface of the silica nanoparticles. Although the separators were dried above 100 °C overnight, there is a complex of hydroxyl and water groups that can only be removed at temperatures exceeding 190 °C. While the particles could be dried beyond such temperatures, the separators they were cast on would suffer degradation. The small amount of water on the surface may be auto-catalyzing the $LiPF_6$ in the electrolyte to form HF over time. Electrode etching over time may explain the decline in capacity.[40]

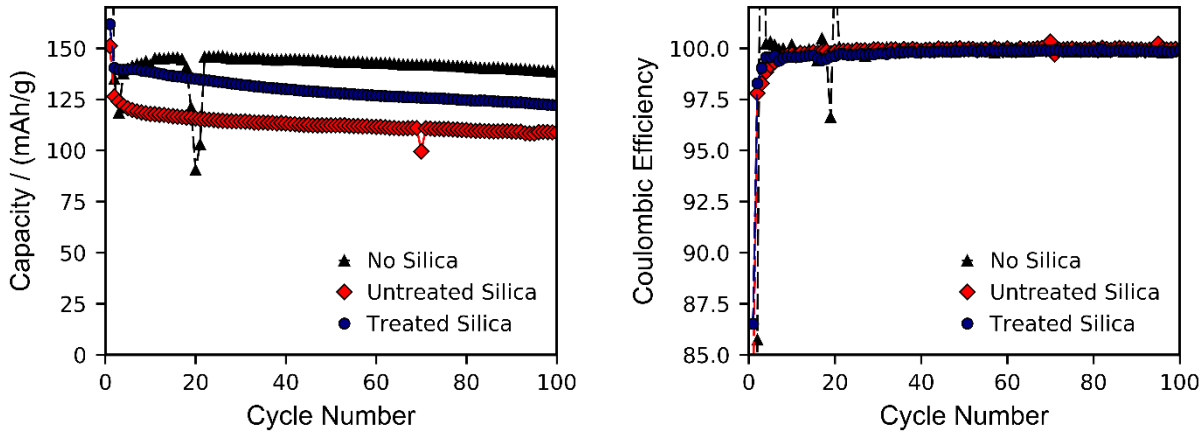

Figure 9. Cycling data for coin cells using shear thickening electrolytes, which were 30 wt.% bare or PMMA-coated silica colloids in 1.2M $LiPF_6$ in 3:7 EC/DMC. Cells with electrolyte containing no silica colloids were used for comparison. Graphite anodes were cycled against NMC cathodes at a cycling rate of C/3 from 3 to 4.2V

To understand how sedimentation affects conductivity over time, interdigitated electrodes (IDEs) were submerged in shear thickening electrolytes (30 wt.% solids, 1.0M $LiPF_6$ in 1:1 EC/DMC v/v). The electrolytes were left to rest at 25 °C for 24 hours. Electrolyte conductivity data as a function of time is given in **Figure 10**. The conductivity of electrolyte with no silica was initially 12.4 mS cm^{-1} and 12.3 mS cm^{-1} after 24 hours. Initial conductivities of electrolytes with particles with bare and PMMA-coated silica nanoparticles were slightly lower, measured at 9.10 and 9.56 mS cm^{-1}, respectively. This was expected as the 30 wt.% solids in electrolyte solution will have a higher viscosity. After 24 hours of rest, conductivities measured for the bare and PMMA coated silica based electrolytes were 1.27 and 7.70 mS cm^{-1}, respectively. Sedimentation is expected to lead to a reduction in electrolyte conductivity measured near IDEs. The increased solid content during sedimentation reduces the fraction of conductive liquid phase and increases the local viscosity near the IDEs, both of which result in decreased conductivity.[39, 41]

Conductivity data revealed that the conductivity of electrolyte with no silica changed little over 24 hours, as expected. Minor fluctuations in conductivity are mostly likely due to temperature changes. Also, as expected, addition of solid non-ionically conducting particles reduced initial conductivity slightly, again due to increased viscosity and reduced conductive phase near the IDEs. However, the change in conductivity of electrolytes with bare and PMMA-coated silica nanoparticles differs greatly over 24 hours as sedimentation is allowed to occur.

The conductivity of electrolytes with bare silica nanoparticles decreases drastically over four hours, suggesting that sedimentation occurred quickly, rapidly increasing local viscosity near the IDE surface. The solution visually appeared to be phase separated. Beyond four hours the conductivity remained low and stable, most likely due to near-complete sedimentation. The conductivity of electrolytes with PMMA coated silica nanoparticles decreases shortly after the initial measurement, most likely due to the electrolyte settling to equilibrium. However, after this period, the conductivity remains relatively high, but stable, an indication that the composition of the dispersion near the interdigitated electrodes is constant. This confirms that the PMMA coating aids in sterically stabilizing the particles and preventing sedimentation.

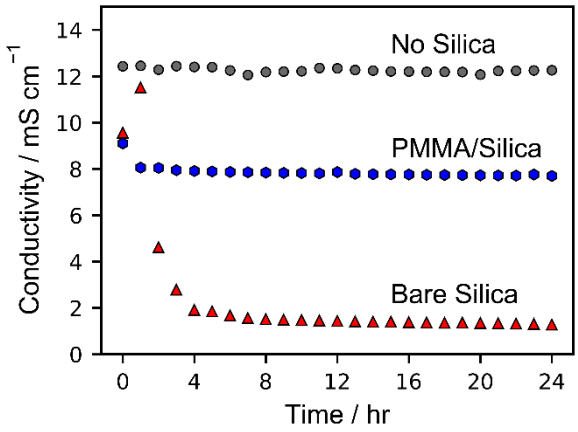

Figure 10. Conductivity of 30 wt% solids in electrolyte (1.0M $LiPF_6$ in 1:1 EC/DMC v/v) as a function of time. At rest, particle sedimentation occurs, affecting conductivity. Interdigitated electrodes were used (cell constant 2 cm^{-1}).

4. Conclusion

In this work, we demonstrate the surface functionalization of silica colloids with PMMA brushes via ATRP for steric stabilization in alkyl carbonate electrolytes used in lithium ion batteries. Improved stabilization of silica nanoparticle colloids was confirmed by *in situ* ultra small angle neutron scattering, rheology, and conductivity measurements. Additionally, our results suggest that introduction of highly concentrated (30 wt. %) shear-thickening electrolytes to lithium ion batteries do not severely adversely affect overall cell capacity. Conductivity of electrolyte with PMMA-coated silica remain quite high, from 9.56 mS cm^{-1} initially to 7.70 mS cm^{-1} after 24 hours at rest, whereas the conductivity of electrolyte with bare silica decreases from 9.10 to 1.27 mS cm^{-1} over the same time period, confirming the PMMA-coating successfully sterically stabilizes the particles in solution at rest. Electrochemical cycling of full lithium ion cells (NMC vs graphite) also confirms that the PMMA-coated silica colloid electrolytes are viable for use in lithium ion batteries, with 86.5% capacity of cells with conventional electrolytes after 100 cycles. Several considerations must be made going forward for proper implementation of shear-thickening electrolytes in lithium ion batteries. PMMA-coated silicon nanoparticles should be dried sufficiently to minimize the presence of water in electrolyte. Drop casting is currently an acceptable technique for small-scale cell assembly. However, an alternative casting method that accommodates the shear-thickening behavior will be necessary for fabrication of larger format cells. Future research will examine the effect of additional parameters on dispersion stabilization and electrochemical performance, such as the size and composition of the colloids and polymer brushes.

AUTHOR INFORMATION

Corresponding Author

***Gabriel M. Veith,** veithgm@ornl.gov

Author Contributions

The manuscript was written through contributions of all authors. BHS fabricated samples, electrochemistry, USANS data collection, rheology. BLA lead the zeta potential measurement and rheology. MD, LH, JFB, MA planned and implemented the USANS study. WET supervised the ATRP synthesis. GMV lead the experimental effort. All authors have given approval to the final version of the manuscript.

Acknowledgments

This material is based upon work supported by the U.S. Department of Energy, Office of Science, Office of Workforce Development for Teachers and Scientists, Office of Science Graduate Student Research (SCGSR) program (BHS). The SCGSR program is administered by the Oak Ridge Institute for Science and Education for the DOE under contract number DE-SC0014664. This work was supported by the National Science Foundation under IGERT award #DGE-0966089 (BHS). A portion of this research used resources at the Spallation Neutron Source, a DOE Office of Science User Facility operated by the Oak Ridge National Laboratory. Small angle scattering measurements were done using the USANS instrument and the Spallation Neutron Source. GMV and BLA were supported by the Advanced Research Projects Agency-Energy (ARPA-E), U.S. Department of Energy, under Award Number DE-AR-0869-1617. The authors thank Tracie Lowe for taking the scanning electron micrograph images. The authors particularly thank Ping Liu, Susan Babinec and Julian Sculley for their helpful discussions. This manuscript has been authored by UT-Battelle, LLC under Contract No. DE-AC05-00OR22725 with the U.S. Department of Energy. The United States Government retains and the publisher, by accepting the article for publication, acknowledges that the United States Government retains a non-exclusive, paid-up, irrevocable, world-wide license to publish or reproduce the published form of this manuscript, or allow others to do so, for United States Government purposes. The Department of Energy will provide public access to these results of federally sponsored research in accordance with the DOE Public Access Plan (http://energy.gov/downloads/doe-public-access-plan).

References

(1) Janek, J.; Zeier, W. G., A solid future for battery development. *Nature Energy* **2016,** *1*, 16141.
(2) Balakrishnan, P. G.; Ramesh, R.; Prem Kumar, T., Safety mechanisms in lithium-ion batteries. *Journal of Power Sources* **2006,** *155* (2), 401-414.
(3) Kato, Y.; Hori, S.; Saito, T.; Suzuki, K.; Hirayama, M.; Mitsui, A.; Yonemura, M.; Iba, H.; Kanno, R., High-power all-solid-state batteries using sulfide superionic conductors. *Nature Energy* **2016,** *1*.
(4) Takada, K., Progress and prospective of solid-state lithium batteries. *Acta Materialia* **2013,** *61* (3), 759-770.
(5) Robinson, A. L.; Janek, J., Solid-state batteries enter EV fray. *MRS Bull.* **2014,** *39* (12), 1046-1047.
(6) Ding, J.; Tian, T.; Meng, Q.; Guo, Z.; Li, W.; Zhang, P.; T Ciacchi, F.; Huang, J.; Yang, W., Smart Multifunctional Fluids for Lithium Ion Batteries: Enhanced Rate Performance and Intrinsic Mechanical Protection. *Scientific Reports* **2013,** *3*, 2485.
(7) Veith, G. M.; Arrnstrong, B. L.; Wang, H.; Kalnaus, S.; Tenhaeff, W. E.; Patterson, M. L., Shear Thickening Electrolytes for High Impact Resistant Batteries. *Acs Energy Letters* **2017,** *2* (9), 2084-2088.
(8) Krishnamurthy, L. N.; Wagner, N. J.; Mewis, J., Shear thickening in polymer stabilized colloidal dispersions. *Journal of Rheology* **2005,** *49* (6), 1347-1360.
(9) Pfaffenhuber, C.; Gobel, M.; Popovic, J.; Maier, J., Soggy-sand electrolytes: status and perspectives. *Physical Chemistry Chemical Physics* **2013,** *15* (42), 18318-18335.
(10) Xu, P.; Wang, H. T.; Tong, R.; Du, Q. G.; Zhong, W., Preparation and morphology of SiO2/PMMA nanohybrids by microemulsion polymerization. *Colloid Polym. Sci.* **2006,** *284* (7), 755-762.
(11) Kobayashi, M.; Juillerat, F.; Galletto, P.; Bowen, P.; Borkovec, M., Aggregation and Charging of Colloidal Silica Particles: Effect of Particle Size. *Langmuir* **2005,** *21* (13), 5761-5769.
(12) Pfaffenhuber, C.; Hoffmann, F.; Froba, M.; Popovic, J.; Maier, J., Soggy-sand effects in liquid composite electrolytes with mesoporous materials as fillers. *Journal of Materials Chemistry A* **2013,** *1* (40), 12560-12567.
(13) Bhattacharyya, A. J., Ion Transport in Liquid Salt Solutions with Oxide Dispersions: "Soggy Sand" Electrolytes. *The Journal of Physical Chemistry Letters* **2012,** *3* (6), 744-750.
(14) Bhattacharyya, A. J.; Maier, J., Second Phase Effects on the Conductivity of Non-Aqueous Salt Solutions: "Soggy Sand Electrolytes". *Advanced Materials* **2004,** *16* (9-10), 811-814.
(15) Das, S. K.; Mandal, S. S.; Bhattacharyya, A. J., Ionic conductivity, mechanical strength and Li-ion battery performance of mono-functional and bi-functional ("Janus") "soggy sand" electrolytes. *Energy Environ. Sci.* **2011,** *4* (4), 1391-1399.
(16) Matyjaszewski, K., Atom Transfer Radical Polymerization (ATRP): Current Status and Future Perspectives. *Macromolecules* **2012,** *45* (10), 4015-4039.
(17) Stejskal, J.; Kratochvíl, P.; Armes, S. P.; Lascelles, S. F.; Riede, A.; Helmstedt, M.; Prokeš, J.; Křivka, I., Polyaniline Dispersions. 6. Stabilization by Colloidal Silica Particles. *Macromolecules* **1996,** *29* (21), 6814-6819.
(18) Hackley, V. A., Colloidal Processing of Silicon Nitride with Poly(acrylic acid): I, Adsorption and Electrostatic Interactions. *Journal of the American Ceramic Society* **1997,** *80* (9), 2315-2325.
(19) Zhang, Z.; Berns, A. E.; Willbold, S.; Buitenhuis, J., Synthesis of poly(ethylene glycol) (PEG)-grafted colloidal silica particles with improved stability in aqueous solvents. *Journal of Colloid and Interface Science* **2007,** *310* (2), 446-455.
(20) Auroy, P.; Auvray, L.; Léger, L., Silica particles stabilized by long grafted polymer chains: From electrostatic to steric repulsion. *Journal of Colloid and Interface Science* **1992,** *150* (1), 187-194.
(21) Manuel Stephan, A.; Nahm, K. S., Review on composite polymer electrolytes for lithium batteries. *Polymer* **2006,** *47* (16), 5952-5964.
(22) Ngai, K. S.; Ramesh, S.; Ramesh, K.; Juan, J. C., A review of polymer electrolytes: fundamental, approaches and applications. *Ionics* **2016,** *22* (8), 1259-1279.
(23) Stober, W.; Fink, A.; Bohn, E., Controlled Growth of Monodisperse Silica Spheres in Micron Size Range. *Journal of Colloid and Interface Science* **1968,** *26* (1), 62-&.
(24) Jousset, S.; Qiu, J.; Matyjaszewski, K.; Granel, C., Atom Transfer Radical Polymerization of Methyl Methacrylate in Water-Borne System. *Macromolecules* **2001,** *34* (19), 6641-6648.

(25) John, M. C.; Michael, A., Aiming for the theoretical limit of sensitivity of Bonse-Hart USANS instruments. *Journal of Physics: Conference Series* **2010,** *251* (1), 012056.
(26) Arnold, O.; Bilheux, J. C.; Borreguero, J. M.; Buts, A.; Campbell, S. I.; Chapon, L.; Doucet, M.; Draper, N.; Leal, R. F.; Gigg, M. A.; Lynch, V. E.; Markvardsen, A.; Mikkelson, D. J.; Mikkelson, R. L.; Miller, R.; Palmen, K.; Parker, P.; Passos, G.; Perring, T. G.; Peterson, P. F.; Ren, S.; Reuter, M. A.; Savici, A. T.; Taylor, J. W.; Taylor, R. J.; Tolchenoy, R.; Zhou, W.; Zikoysky, J., Mantid-Data analysis and visualization package for neutron scattering and mu SR experiments. *Nuclear Instruments & Methods in Physics Research Section a-Accelerators Spectrometers Detectors and Associated Equipment* **2014,** *764*, 156-166.
(27) Doucet, M. C., Jae Hie; Alina, Gervaise; King, Stephen; Butler, Paul; Kienzle, Paul; Krzywon, Jeff; Jackson, Andrew; Richter, Tobias; Gonzales, Miguel; Nielsen, Torben; Ferraz Leal, Ricardo; Markvardsen, Anders; Heenan, Richard; Juhas, Pavol; Bakker, Jurrian; Rozyczko, Piotr; Potrzebowski, Wojciech; O'driscoll, Lewis; Campbell, Kieran; Washington, Adam SasView Version 4.0. http://doi.org/10.5281/zenodo.159083.
(28) Potapov, V. V.; Zhuravlev, L. T., Temperature Dependence of the Concentration of Silanol Groups in Silica Precipitated from a Hydrothermal Solution. *Glass Physics and Chemistry* **2005,** *31* (5), 661-670.
(29) Zhao, B., A Combinatorial Approach to Study Solvent-Induced Self-Assembly of Mixed Poly(methyl methacrylate)/Polystyrene Brushes on Planar Silica Substrates: Effect of Relative Grafting Density. *Langmuir* **2004,** *20* (26), 11748-11755.
(30) Xu, Y.; Thurber, C. M.; Macosko, C. W.; Lodge, T. P.; Hillmyer, M. A., Poly(methyl methacrylate)-block-polyethylene-block-poly(methyl methacrylate) Triblock Copolymers as Compatibilizers for Polyethylene/Poly(methyl methacrylate) Blends. *Industrial & Engineering Chemistry Research* **2014,** *53* (12), 4718-4725.
(31) Mawhinney, D. B.; Glass, J. A.; Yates, J. T., FTIR Study of the Oxidation of Porous Silicon. *The Journal of Physical Chemistry B* **1997,** *101* (7), 1202-1206.
(32) Dirlikov, S.; Koenig, J. L., Infrared Spectra of Poly(Methyl Methacrylate) Labeled with Oxygen-18. *Applied Spectroscopy* **1979,** *33* (6), 551-555.
(33) Catalano, F.; Alberto, G.; Ivanchenko, P.; Dovbeshko, G.; Martra, G., Effect of Silica Surface Properties on the Formation of Multilayer or Submonolayer Protein Hard Corona: Albumin Adsorption on Pyrolytic and Colloidal SiO2 Nanoparticles. *The Journal of Physical Chemistry C* **2015,** *119* (47), 26493-26505.
(34) Lotfizadeh, S.; Aljama, H.; Reilly, D.; Matsoukas, T., Formation of Reversible Clusters with Controlled Degree of Aggregation. *Langmuir* **2016,** *32* (19), 4862-4867.
(35) Bagwe, R. P.; Hilliard, L. R.; Tan, W. H., Surface modification of silica nanoparticles to reduce aggregation and nonspecific binding. *Langmuir* **2006,** *22* (9), 4357-4362.
(36) Muzny, C. D.; Butler, B. D.; Hanley, H. J. M.; Agamalian, M., An ultra-small-angle neutron scattering study of the restructuring of sheared colloidal silica gels. *Journal of Physics: Condensed Matter* **1999,** *11* (26), L295.
(37) Kawaguchi, M.; Ryo, Y.; Hada, T., Rheological properties of silica suspensions in aqueous cellulose derivative solutions. 1. Viscosity measurements. *Langmuir* **1991,** *7* (7), 1340-1343.
(38) Kim, U.-H.; Lee, E.-J.; Yoon, C. S.; Myung, S.-T.; Sun, Y.-K., Compositionally Graded Cathode Material with Long-Term Cycling Stability for Electric Vehicles Application. *Advanced Energy Materials* **2016,** *6* (22), 1601417-n/a.
(39) Southall, J. P.; Hubbard, H.; Johnston, S. F.; Rogers, V.; Davies, G. R.; McIntyre, J. E.; Ward, I. M., Ionic conductivity and viscosity correlations in liquid electrolytes for incorporation into PVDF gel electrolytes. *Solid State Ionics* **1996,** *85* (1-4), 51-60.
(40) Xu, J.; Deshpande, R. D.; Pan, J.; Cheng, Y.-T.; Battaglia, V. S., Electrode Side Reactions, Capacity Loss and Mechanical Degradation in Lithium-Ion Batteries. *Journal of The Electrochemical Society* **2015,** *162* (10), A2026-A2035.
(41) Shen, B. H.; Veith, G. M.; Armstrong, B. L.; Tenhaeff, W. E.; Sacci, R. L., Predictive Design of Shear-Thickening Electrolytes for Safety Considerations. *Journal of The Electrochemical Society* **2017,** *164* (12), A2547-A2551.

SYNOPSIS TOC (Word Style "SN_Synopsis_TOC"). If you are submitting your paper to a journal that requires a synopsis graphic and/or synopsis paragraph, see the Instructions for Authors on the journal's homepage for a description of what needs to be provided and for the size requirements of the artwork.

To format double-column figures, schemes, charts, and tables, use the following instructions:

Place the insertion point where you want to change the number of columns
From the **Insert** menu, choose **Break**
Under **Sections**, choose **Continuous**
Make sure the insertion point is in the new section. From the **Format** menu, choose **Columns**
In the **Number of Columns** box, type **1**
Choose the **OK** button

Now your page is set up so that figures, schemes, charts, and tables can span two columns. These must appear at the top of the page. Be sure to add another section break after the table and change it back to two columns with a spacing of 0.33 in.

Table 1. Example of a Double-Column Table

Column 1	Column 2	Column 3	Column 4	Column 5	Column 6	Column 7	Column 8

Authors are required to submit a graphic entry for the Table of Contents (TOC) that, in conjunction with the manuscript title, should give the reader a representative idea of one of the following: A key structure, reaction, equation, concept, or theorem, etc., that is discussed in the manuscript. Consult the journal's Instructions for Authors for TOC graphic specifications.

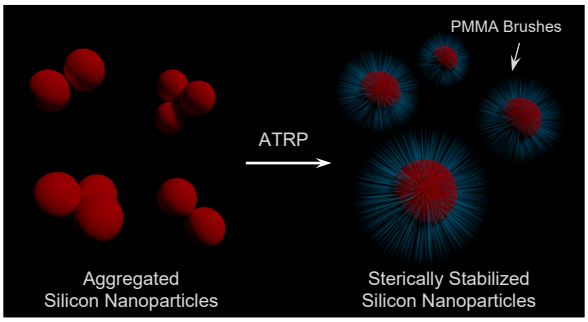

Insert Table of Contents artwork here